Gamma-Ray Observation of the Cygnus Region in the 100-TeV Energy Region

M. Amenomori,[1] Y. W. Bao,[2] X. J. Bi,[3] D. Chen,[4,*] T. L. Chen,[5] W. Y. Chen,[3] Xu Chen,[3] Y. Chen,[2] Cirennima,[5] S. W. Cui,[6] Danzengluobu,[5] L. K. Ding,[3] J. H. Fang,[3,7] K. Fang,[3] C. F. Feng,[8] Zhaoyang Feng,[3] Z. Y. Feng,[9] Qi Gao,[5] A. Gomi,[10] Q. B. Gou,[3] Y. Q. Guo,[3] Y. Y. Guo,[3] H. H. He,[3] Z. T. He,[6] K. Hibino,[11] N. Hotta,[12] Haibing Hu,[5] H. B. Hu,[3] J. Huang,[3,†] H. Y. Jia,[9] L. Jiang,[3] P. Jiang,[4] H. B. Jin,[4] K. Kasahara,[13] Y. Katayose,[10] C. Kato,[14] S. Kato,[15] K. Kawata,[15] M. Kozai,[16] D. Kurashige,[10] Labaciren,[5] G. M. Le,[17] A. F. Li,[18,8,3] H. J. Li,[5] W. J. Li,[3,9] Y. Li,[4] Y. H. Lin,[3,7] B. Liu,[19] C. Liu,[3] J. S. Liu,[3] L. Y. Liu,[4] M. Y. Liu,[5] W. Liu,[3] X. L. Liu,[4] Y.-Q. Lou,[20,21,22] H. Lu,[3] X. R. Meng,[5] K. Munakata,[14] H. Nakada,[10] Y. Nakamura,[3,15] Y. Nakazawa,[23] H. Nanjo,[1] C. C. Ning,[5] M. Nishizawa,[24] M. Ohnishi,[15] T. Ohura,[10] S. Okukawa,[10] S. Ozawa,[25] L. Qian,[4] X. Qian,[4] X. L. Qian,[26] X. B. Qu,[27] T. Saito,[28] M. Sakata,[29] T. Sako,[15] T. K. Sako,[15,‡] J. Shao,[3,8] M. Shibata,[10] A. Shiomi,[23] H. Sugimoto,[30] W. Takano,[11] M. Takita,[15,§] Y. H. Tan,[3] N. Tateyama,[11] S. Torii,[31] H. Tsuchiya,[32] S. Udo,[11] H. Wang,[3] Y. P. Wang,[5] Wangdui,[5] H. R. Wu,[3] Q. Wu,[5] J. L. Xu,[4] L. Xue,[8] Y. Yamamoto,[29,‖] Z. Yang,[3] Y. Q. Yao,[4] J. Yin,[4] Y. Yokoe,[15] N. P. Yu,[4] A. F. Yuan,[5] L. M. Zhai,[4] C. P. Zhang,[4] H. M. Zhang,[3] J. L. Zhang,[3] X. Zhang,[2] X. Y. Zhang,[8] Y. Zhang,[3] Yi Zhang,[33] Ying Zhang,[3] S. P. Zhao,[3] Zhaxisangzhu,[5] and X. X. Zhou[9]

(Tibet AS$_\gamma$ Collaboration)

[1]*Department of Physics, Hirosaki University, Hirosaki 036-8561, Japan*
[2]*School of Astronomy and Space Science, Nanjing University, Nanjing 210093, China*
[3]*Key Laboratory of Particle Astrophysics, Institute of High Energy Physics, Chinese Academy of Sciences, Beijing 100049, China*
[4]*National Astronomical Observatories, Chinese Academy of Sciences, Beijing 100012, China*
[5]*Department of Mathematics and Physics, Tibet University, Lhasa 850000, China*
[6]*Department of Physics, Hebei Normal University, Shijiazhuang 050016, China*
[7]*University of Chinese Academy of Sciences, Beijing 100049, China*
[8]*Institute of Frontier and Interdisciplinary Science and Key Laboratory of Particle Physics and Particle Irradiation (MOE), Shandong University, Qingdao 266237, China*
[9]*Institute of Modern Physics, SouthWest Jiaotong University, Chengdu 610031, China*
[10]*Faculty of Engineering, Yokohama National University, Yokohama 240-8501, Japan*
[11]*Faculty of Engineering, Kanagawa University, Yokohama 221-8686, Japan*
[12]*Faculty of Education, Utsunomiya University, Utsunomiya 321-8505, Japan*
[13]*Faculty of Systems Engineering, Shibaura Institute of Technology, Omiya 330-8570, Japan*
[14]*Department of Physics, Shinshu University, Matsumoto 390-8621, Japan*
[15]*Institute for Cosmic Ray Research, University of Tokyo, Kashiwa 277-8582, Japan*
[16]*Institute of Space and Astronautical Science, Japan Aerospace Exploration Agency (ISAS/JAXA), Sagamihara 252-5210, Japan*
[17]*National Center for Space Weather, China Meteorological Administration, Beijing 100081, China*
[18]*School of Information Science and Engineering, Shandong Agriculture University, Taian 271018, China*
[19]*Department of Astronomy, School of Physical Sciences, University of Science and Technology of China, Hefei, Anhui 230026, China*
[20]*Department of Physics and Tsinghua Centre for Astrophysics (THCA), Tsinghua University, Beijing 100084, China*
[21]*Tsinghua University-National Astronomical Observatories of China (NAOC) Joint Research Center for Astrophysics, Tsinghua University, Beijing 100084, China*
[22]*Department of Astronomy, Tsinghua University, Beijing 100084, China*
[23]*College of Industrial Technology, Nihon University, Narashino 275-8575, Japan*
[24]*National Institute of Informatics, Tokyo 101-8430, Japan*
[25]*National Institute of Information and Communications Technology, Tokyo 184-8795, Japan*
[26]*Department of Mechanical and Electrical Engineering, Shangdong Management University, Jinan 250357, China*
[27]*College of Science, China University of Petroleum, Qingdao 266555, China*
[28]*Tokyo Metropolitan College of Industrial Technology, Tokyo 116-8523, Japan*
[29]*Department of Physics, Konan University, Kobe 658-8501, Japan*
[30]*Shonan Institute of Technology, Fujisawa 251-8511, Japan*
[31]*Research Institute for Science and Engineering, Waseda University, Tokyo 162-0044, Japan*
[32]*Japan Atomic Energy Agency, Tokai-mura 319-1195, Japan*
[33]*Key Laboratory of Dark Matter and Space Astronomy, Purple Mountain Observatory, Chinese Academy of Sciences, Nanjing 210034, China*

We report observations of gamma-ray emissions with energies in the 100-TeV energy region from the Cygnus region in our Galaxy. Two sources are significantly detected in the directions of the Cygnus OB1 and OB2 associations. Based on their positional coincidences, we associate one with a pulsar PSR J2032 + 4127 and the other mainly with a pulsar wind nebula PWN G75.2 + 0.1, with the pulsar moving away from its original birthplace situated around the centroid of the observed gamma-ray emission. This work would stimulate further studies of particle acceleration mechanisms at these gamma-ray sources.

Introduction.—The Cygnus region is a large active star-forming complex in our Galaxy, hosting numerous pulsar wind nebulae (PWNe) and supernova remnants (SNRs) as well as Wolf-Rayet stars, OB associations, open clusters, etc. This region is a natural laboratory to study cosmic-ray acceleration and transport and has been observed in various wavebands. Especially interesting in light of TeV gamma-ray observations are the Cygnus OB1 and OB2 associations.

In the direction of Cygnus OB2, the HEGRA imaging air Cherenkov telescope (IACT) discovered a gamma-ray source TeV J2032 + 4130 [1,2], and follow-up observations have been made via other IACTs including Whipple [3], MAGIC [4], and VERITAS [5,6]. They reported gamma-ray fluxes of roughly 3% that of the Crab nebula above 1 TeV and source extensions of radii 0.1°–0.2°. Meanwhile, air-shower arrays generally reported fluxes much higher than those of IACTs at multi-TeV energies [7–11]. For example, ARGO [9] employed a larger variable-size window with a radius of approximately 1.5° at 1 TeV and reported flux data points 5–10 times those of IACTs at multi-TeV energies, and the flux reported at 7 TeV by HAWC with a window of radius 0.7° was approximately twice that based on their point-source analysis [11], which appears to be consistent with the IACT measurements. A recent HAWC article [12] reported that there is a largely extended "Cocoon" region (HAWC J2030 + 409) with a Gaussian width of 2.13°, counterpart of the GeV Cygnus Cocoon [13], underneath the gamma-ray emission of HAWC J2031 + 415 with a width of 0.27°, counterpart of TeV J2032 + 4130. A plausible explanation of the discrepancy in the measured fluxes between IACTs and air-shower arrays is that IACTs extract the emission of HAWC J2031 + 415 by counting the extended emission of the Cocoon region in estimating the background, while air-shower arrays tend to integrate part of the gamma-ray emission of the Cocoon region inside their relatively large window sizes as well as the gamma-ray emission of HAWC J2031 + 415. Additionally, HAWC detected eHWC J2030 + 412 above 56 TeV with an extension of 0.18° [14], although the association of eHWC J2030 + 412 with TeV J2032 + 4130/PSR J2032 + 4127 is a matter of debate, given that eHWC J2030 + 412 is 0.36° away from TeV J2032 + 4130 and 0.33° away from PSR J2032 + 4127.

Located 0.18° southeast of the centroid of TeV J2032 + 4130 is the radio pulsar PSR J2032 + 4127, with a distance from Earth of 1.4–1.7 kpc [15–17], a characteristic age of 180 kyr, and a spin-down luminosity of 1.7×10^{35} erg/s [18]. PSR J2032 + 4127 forms a binary system with a massive B0Ve star MT91 213, and a flux enhancement of this binary system in the 2017 autumn periastron period was observed at the 0.2–2 TeV energy region by VERITAS and MAGIC and at the 0.3–10 keV energy region by the Swift x-ray telescope and NuSTAR [19–21].

In the direction of Cygnus OB1, a gamma-ray source MGRO J2019 + 37 was discovered by Milagro at the median energy of 12 TeV with a source extension of 0.3° [22], and this source was also recently observed by HAWC [14,23]. VERITAS observed the same region above 0.6 TeV and separated the gamma-ray emissions into two sources: VER J2019 + 368 and VER J2016 + 371 [24]. VERITAS also reported that the morphology of VER J2019 + 368 is asymmetrical with $\sigma_{major}(\sigma_{minor}) \approx 0.34°$ (0.13°). The flux of VER J2019 + 368 measured by VERITAS in 2014 [24] is a few times higher than that in 2018 [6] because of different collection areas of photon integration windows.

Located 0.36° east of the centroid of VER J2019 + 368 is the radio pulsar PSR J2021 + 3651, having a characteristic age of 17 kyr and a spin-down luminosity of 3.4×10^{36} erg/s [25]. PSR J2021 + 3651 is one of the relatively few pulsars that have gamma-ray pulsations observed by Fermi-LAT [26]. The distance D to the pulsar has remained a matter of debate. $D \sim 12$ kpc was suggested by the dispersion measure [25] and $D \geq 5$ kpc by the pulsar polarization rotation measure [26]. Comparing the HI column density along the pulsar line of sight with the hydrogen absorbing column density implied $D \sim 10$ kpc [27] or 3–4 kpc [28], and $D = 1.8^{+1.7}_{-1.4}$ kpc was obtained from the absorption-distance relation using red-clump stars in the direction of the pulsar [29]. This value is consistent with 1.58 kpc, which is the estimated distance to Cygnus OB1 [30,31]. PSR J2021 + 3651 appears to form a pulsar wind nebula referred to as PWN G75.2 + 0.1 [27], and the radio and x-ray morphologies of this nebula feature a bright bow-shaped tail extending westward from the pulsar, indicating that the pulsar is moving eastward with its birthplace as far west as the apparent end of the tail at $\approx 0.2°$ west of the current pulsar position [24,32]. In

addition, a number of hard x-ray sources were identified along the western edge of VER J2019 + 368 by NuSTAR space observations including a young massive stellar cluster [33].

Experiment and data analysis.—The Tibet air-shower (AS) array has been observing cosmic rays and gamma rays above TeV energies since 1990 at Yangbajing (90.522 °E, 30.102 °N; 4300 m above sea level) in Tibet, China [34]. In this work, we use data obtained by the Tibet AS array combined with the muon detector array during 719 live days from February 2014 to May 2017. Our data analysis method and data selection criteria as well as the array configuration are the same as described in our previous articles [35,36]. We use the equi-zenith-angle method [37] to estimate the gamma-ray excess count and the number of background events. Twenty OFF regions are taken, and the radius of the analysis window is variable depending on the recorded air-shower size from approximately 0.7° at lower energies around 10 TeV to a lower limit of 0.5°.

In the following section, we discuss two gamma-ray sources detected significantly above 10 TeV in the directions of Cygnus OB1 and OB2, respectively.

Results and discussion.—Cygnus OB2: Figure 1(a) shows a detection significance map around the gamma-ray source detected by this work with photon energies above 10 TeV in the direction of Cygnus OB2. The sky is gridded in $0.1° \times 0.1°$ pixels and the significance value of each pixel calculated according to [38] is smoothed by a circular search window of radius R_w centered at the pixel. Assuming a symmetrical 2D Gaussian distribution for the gamma-ray excess, we fit the events within the $4° \times 4°$ region around the source using the unbinned maximum likelihood method. The centroid of gamma-ray emissions detected at the pretrial (post-trial) detection significance of 5.3σ (4.7σ) above 10 TeV is estimated at $(\text{R.A.}, \text{Dec.}) = (308.04° \pm 0.08°, 41.46° \pm 0.06°)$. We name this source TASG J2032 + 414. The location of TASG J2032 + 414 is in good agreement with that of the pulsar PSR J2032 + 4127 and consistent with that of HAWC J2031 + 415 [12] at the 1.7σ level, while it appears to deviate from that of TeV J2032 + 4130 reported in [20] at the 2.8σ level. We also find that most of the gamma-ray emission detected above 10 TeV is confined inside a void where the radio (frequency 1420 MHz) [39] and infrared (wavelength 24 μm) [40,41] emissions are very weak. This morphology was also seen by VERITAS [6].

Figure 2(a) shows the distribution of the number of observed events above 10 TeV as a function of the square of the opening angle ϕ between the estimated arrival direction and the TASG J2032 + 414 centroid. To estimate a possible source extension, we perform the χ^2 fitting of the data with the function $A \exp[-\phi^2/2(\sigma_{PSF}^2 + \sigma_{EXT}^2)] + N_{BG}$, where A and σ_{EXT} are two fitting parameters and $\sigma_{PSF} = 0.36°$ and $N_{BG} = 224.5$ are the point spread function (PSF) of our instrument above 10 TeV and the number of background

events estimated from the background cosmic-ray data, we get $\sigma_{EXT} = 0.00° \pm 0.14°$, which is consistent with that obtained from the maximum likelihood fitting described above. The χ^2/ndf of the fitting is 33.8/38. With a large error of 0.14°, the σ_{EXT} value above 10 TeV does not
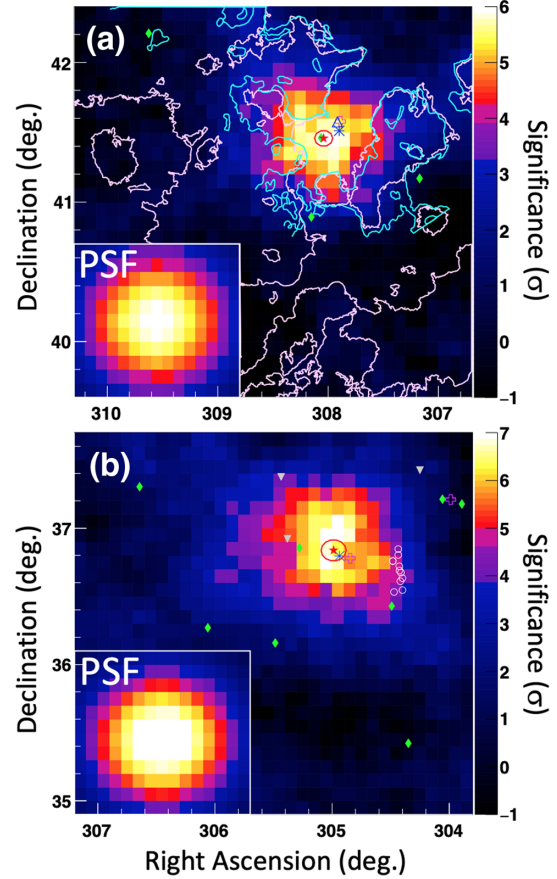

FIG. 1. Significance maps around the two gamma-ray emission sources detected above 10 TeV in the directions of Cygnus OB2 (a) and OB1 (b), smoothed by search windows (see the text). The point spread function (PSF) is shown in the inset figure. The red filled star with a position error circle is the centroid of TASG J2032 + 414-TASG J2019 + 368 obtained by this work, while the magenta open cross is the centroid of VER J2031 + 415 [20] in (a) and VER J2019 + 368 [6] in (b) and the blue asterisk is that of HAWC J2031 + 415 [12] in (a) and 3HWC J2019 + 367 [23] in (b). The green filled diamonds show Fermi-LAT sources [42]. (a) The blue open triangle indicates the centroid of MAGIC J2031 + 4134 [20]. The green filled diamond coincident with our gamma-ray emission centroid is the pulsar PSR J2032 + 4127. The sky-blue contours indicate 1420 MHz radio emissions provided by the Canadian Galactic Plane Survey [39], and the pink contours indicate 24 μm infrared emissions by the Cygnus-X Spitzer Legacy Survey [40,41]. (b) The white open circles are NuSTAR x-ray sources [33], and the gray filled inverted triangles are Wolf-Rayet stars [43]. The green filled diamond located at 0.23° east of our emission centroid is the pulsar PSR J2021 + 3651. The magenta open cross located at $(\text{R.A.}, \text{Dec.}) = (303.99°, 37.21°)$ is another VERITAS source VER J2016 + 371 [6], which is not detected significantly in this work.
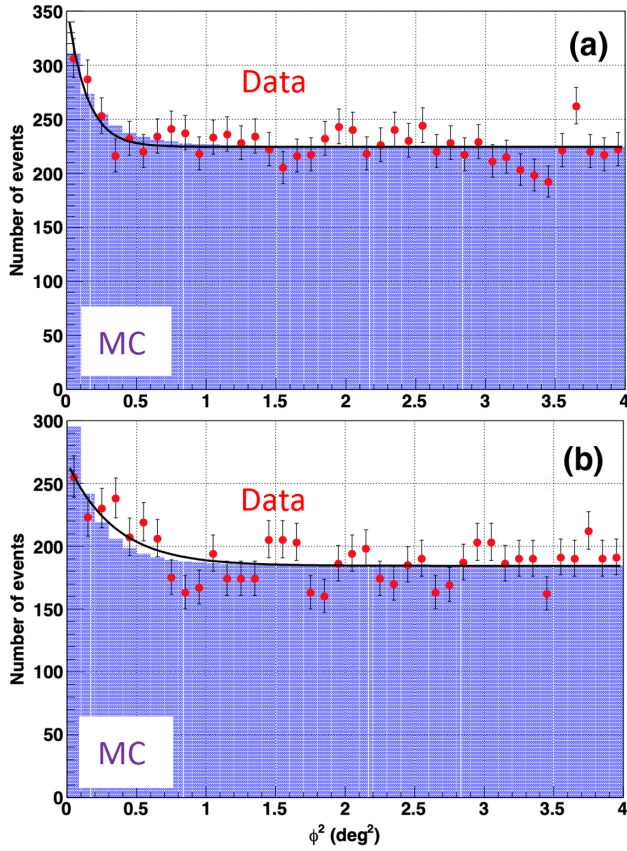
FIG. 2. Number of events observed with photon energies above 10 TeV as a function of the square of the opening angle between the estimated arrival direction and the centroid of TASG J2032 + 414 in (a) and TASG J2019 + 368 in (b). The red filled circles are the experimental data, with the best-fit Gaussian function indicated by the solid line. The blue histogram is the distribution of events expected by the MC simulation assuming a point-like gamma-ray source.

indicate whether TASG J2032 + 414 is extended or not even though it is consistent with the previous measurements at multi-TeV energies by IACTs, ARGO, and HAWC within the 2σ level [2–4,6,9,12,20].

At higher energies above 40 TeV, our source location is consistent with that of PSR J2032 + 4127, and the estimated value of $\sigma_{EXT} = 0.16° \pm 0.09°$ suggests a slight source extension at the 1.9σ level (refer to Supplemental Material [44], Figs. S1 and S2). There seems to be a tension between the centroid of our source above 40 TeV and that of eHWC J2030 + 412 above 56 TeV [14] at a statistical significance of 3.5σ, which might result from the complex morphology of the Cygnus Cocoon region, as these source locations are obtained under the assumption of a Gaussian spatial distribution for gamma-ray signals.

Figure 3(a) shows the differential energy spectrum of TASG J2032 + 414 (red filled squares and downward arrows). Although there is a discrepancy in flux at multi-TeV energies as explained in the Introduction, our flux data points above 10 TeV are consistent with previous
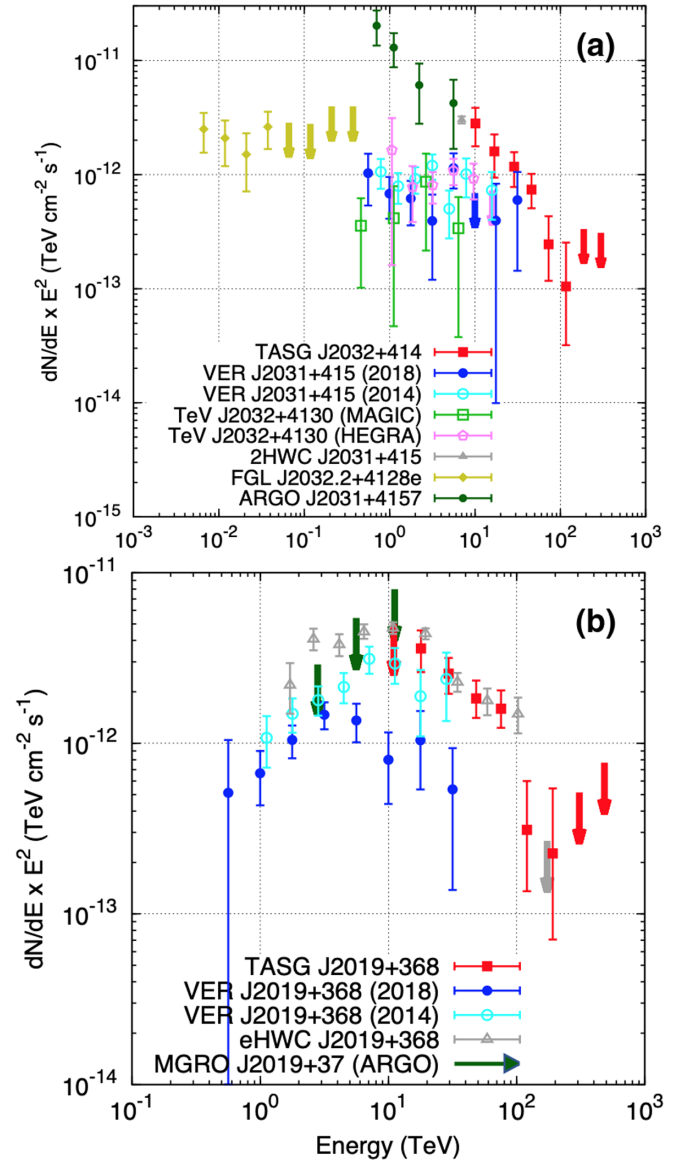

FIG. 3. Differential gamma-ray energy spectra of (a) TASG J2032 + 414 and (b) TASG J2019 + 368 with 95% C.L. upper limits measured by this work (red filled squares/arrows). In both panels, the blue filled circles/arrow (sky-blue open circles) show the gamma-ray spectrum of reported by VERITAS in 2018 (2014) [5,6,24], the gray open triangles/arrow by HAWC [11,14], and the dark-green filled circles/arrows by ARGO [9]. Additionally in panel (a), the gold filled diamonds are reported by Fermi-LAT [6], the green open squares by MAGIC [4], and the pink pentagons/arrow by HEGRA [2]. The upper limits of Fermi-LAT, HAWC, and VERITAS are at the 95% confidence level, while those of HEGRA in (a) and ARGO in (b) are at the 99% and 90% confidence levels, respectively.

measurements of IACTs when the spillover of gamma-ray signals outside their integration radius is taken into account. Our spectrum from 10 TeV to 120 TeV can be expressed by a simple power law as $dF/dE = N_0(E/40 \text{ TeV})^{-\Gamma}$, where $N_0 = (4.13 \pm 0.83) \times 10^{-16} \text{ TeV}^{-1} \text{ cm}^{-2} \text{ s}^{-1}$ is the differential gamma-ray flux

at 40 TeV and $\Gamma = 3.12 \pm 0.21$ is the spectral index ($\chi^2/\mathrm{ndf} = 1.6/4$).

Given that the TASG J2032 + 414 centroid is in good agreement with the location of the radio pulsar PSR J2032 + 4127, the observed gamma rays would be produced by relativistic electrons injected by the pulsar through the inverse-Compton scattering (ICS) with synchrotron and ambient photons. Unfortunately, the time span of our data does not cover the 2017 autumn periastron period of the binary system PSR J2032 + 4127-MT91 213. TASG J2032 + 414, therefore, is considered to be associated with the pulsar itself rather than with the whole binary system. VERITAS and MAGIC detected TeV gamma-ray emissions coincident with TeV J2032 + 4130, which is considered to be the pulsar wind nebula of PSR J2032 + 4127 with its centroid 0.2° away from the location of PSR J2032 + 4127. If the pulsar is moving in the southeast direction along the elongation of the TeV gamma-ray emission as suggested in [5], it would be natural to consider that gamma rays above 10 TeV produced by parent electrons with energies of $\gtrsim 100$ TeV are confined around the current pulsar location, while parent electrons of TeV gamma rays were accelerated earlier when the pulsar was at the centroid of TeV J2032 + 4130.

The other two TeV sources reported earlier in this region, VER J2019 + 407-3HWC J2020 + 403 and 2HWC J2024 + 417*, are not significantly detected in this work. We obtain 99% C.L. integral flux upper limits above 10 TeV (100 TeV) of 1.0×10^{-13} cm^{-2} s^{-1} (1.7×10^{-15} cm^{-2} s^{-1}) for VER J2019 + 407-3HWC J2020+403, and 0.92×10^{-13} cm^{-2} s^{-1} (2.0×10^{-15} cm^{-2} s^{-1}) for 2HWC J2024 + 417*.

Cygnus OB1: Figure 1(b) shows a significance map above 10 TeV in the direction of Cygnus OB1 obtained by this work. The centroid of gamma-ray emissions is estimated at (R.A., Dec.) = (304.99° ± 0.11°, 36.84° ± 0.08°) with the pretrial (post-trial) detection significance of 6.7σ (6.2σ). We name this source TASG J2019 + 368. The centroid of TASG J2019 + 368 is consistent with that reported by HAWC [23] within the 1σ level and by VERITAS [6] within the 2σ level. Possible particle acceleration sites are also indicated in the figure: NuSTAR x-ray sources [33], Wolf-Rayet stars [43], and Fermi-LAT sources [42]. The pulsar PSR J2021 + 3651, located 0.23° east of the TASG J2019 + 368 centroid, has a nebula extending westward from the pulsar, PWN G75.2 + 0.1, which is coincident with the location of TASG J2019 + 368.

Figure 2(b) shows the ϕ^2 distribution of the events observed above 10 TeV. The experimental data can be fitted with a Gaussian function with a source extension of $\sigma_{\mathrm{EXT}} = 0.28° \pm 0.07°$ above 10 TeV, consistent with the extension reported by VERITAS [6] (HAWC [14]) at the 2.1σ (0.3σ) level. The χ^2/ndf of the fitting is 49.1/38.

At higher energies above 40 TeV, our source location is consistent with that of VERITAS [6] and HAWC [14,23], and the estimated value of $\sigma_{\mathrm{EXT}} = 0.22° \pm 0.05°$ suggests that the extension could become smaller as photon energy increases (refer to Supplemental Material [44], Figs. S1 and S2). This tendency was also seen earlier by HAWC [14] [$\sigma_{\mathrm{EXT}} = 0.30° \pm 0.02°(0.20° \pm 0.05°)$ above ~ 1 TeV (56 TeV)].

Figure 3(b) shows the differential gamma-ray energy spectrum of TASG J2019 + 368, which is in good agreement with the HAWC spectrum and consistently connects with the VERITAS spectrum reported in 2014. Our spectrum can be expressed either as $dF/dE = N_0(E/40 \text{ TeV})^{-\Gamma}$, with $N_0 = (10.6 \pm 1.3) \times 10^{-16}$ TeV^{-1} cm^{-2} s^{-1} and $\Gamma = 2.70 \pm 0.13$ ($\chi^2/\mathrm{ndf} = 10.4/5$), or including an exponential cutoff as $dF/dE = N_0(E/40 \text{ TeV})^{-\Gamma} \exp(-E/E_{\mathrm{cut}})$, with $N_0 = (3.6 \pm 2.0) \times 10^{-15}$ TeV^{-1} cm^{-2} s^{-1}, $\Gamma = 1.6 \pm 0.5$, and $E_{\mathrm{cut}} = 44 \pm 21$ TeV ($\chi^2/\mathrm{ndf} = 3.0/4$). The latter fitting is preferred because the best-fit power-law function of the former fitting conflicts with the HAWC upper limit at 170 TeV.

The current position of the pulsar PSR J2021 + 3651 is 0.23° east of our gamma-ray emission centroid, and the estimated location of the pulsar's birthplace resides in our 1σ position error circle, indicating that the gamma-ray emission observed above 10 TeV by this work would be mainly caused by relativistic electrons produced by PSR J2021 + 3651 around the time when the pulsar was very young. If the pulsar birthplace is the gamma-ray emission centroid obtained by this work, the transverse velocity of the pulsar can be expressed as $v = 420(D/1.8 \text{ kpc})(\tau/17 \text{ kyr})^{-1}$ km/s, where τ is the pulsar age. Among known pulsar velocities [45], $v = 420$ km/s is a plausible value. We consider that the observed gamma-ray emission is associated mainly with PSR J2021 + 3651, although there might be some contributions from nearby sources such as the NuSTAR sources.

The other TeV source VER J2016 + 371 reported earlier in this region is not significantly detected by this work. We obtain a 99% C.L. integral flux upper limit above 10 TeV (100 TeV) of 0.91×10^{-13} cm^{-2} s^{-1} (1.4×10^{-15} cm^{-2} s^{-1}) for VER J2016 + 371.

Conclusions.—Using the Tibet air shower array combined with the underground muon detector array, we have detected two gamma-ray sources in the direction of the Cygnus region significantly with photon energies above 10 TeV: TASG J2032 + 414 in the direction of Cygnus OB2 at (R.A., Dec.) = (308.04° ± 0.08°, 41.46° ± 0.06°)), coincident with PSR J2032 + 4127 and TASG J2019 + 368 in the direction of Cygnus OB1 at (R.A., Dec.) = (304.99° ± 0.11°, 36.84° ± 0.08°), coincident with PWN G75.2 + 0.1.

We provide for the first time flux data points from 40 TeV to 120 TeV for the gamma-ray emission region in

the direction of Cygnus OB2, and we confirm the HAWC spectrum up to 100 TeV and provide flux data points from 120 TeV to 200 TeV for the gamma-ray emission region in the direction of Cygnus OB1. For both cases, the observed gamma-ray emissions likely result from relativistic electrons injected by the pulsar through the ICS with synchrotron and ambient photons. PSR J2021 + 3651 could be moving eastward with a velocity of ∼400 km/s away from its original birthplace situated around the observed gamma-ray emission centroid. Future observations and theoretical studies would shed more light on the physical mechanisms of particle acceleration at these two high-energy gamma-ray sources.

---

[*]chending@bao.ac.cn
[†]huangjing@ihep.ac.cn
[‡]tsako@icrr.u-tokyo.ac.jp
[§]takita@icrr.u-tokyo.ac.jp
[‖]Deceased

[1] F. Aharonian *et al.*, Astron. Astrophys. **393,** L37 (2002).
[2] F. Aharonian *et al.*, Astron. Astrophys. **431,** 197 (2005).
[3] A. Konopelko *et al.*, Astrophys. J. **658,** 1062 (2007).
[4] J. Albert *et al.*, Astrophys. J. Lett. **675,** L25 (2008).
[5] E. Aliu *et al.*, Astrophys. J. **783,** 16 (2014).
[6] A. U. Abeysekara *et al.*, Astrophys. J. **861,** 134 (2018).
[7] A. A. Abdo *et al.*, Astrophys. J. Lett. **664,** L91 (2007).
[8] A. A. Abdo *et al.*, Astrophys. J. **753,** 159 (2012).
[9] B. Bartoli *et al.*, Astrophys. J. Lett. **745,** L22 (2012).
[10] B. Bartoli *et al.*, Astrophys. J. **790,** 152 (2014).
[11] A. U. Abeysekara *et al.*, Astrophys. J. **843,** 40 (2017).
[12] A. U. Abeysekara *et al.*, Nat. Astron. Lett. **5,** 465 (2021).
[13] M. Ackermann *et al.*, Science **334,** 1103 (2011).
[14] A. U. Abeysekara *et al.*, Phys. Rev. Lett. **124,** 021102 (2020).
[15] P. Massey and A. B. Thompson, Astron. J. **101,** 1408 (1991).
[16] M. M. Hanson, Astrophys. J. **597,** 957 (2003).
[17] K. L. J. Rygl, A. Brunthaler, A. Sanna, K. M. Menten, M. J. Reid, H. J. van Langevelde, M. Honma, K. J. E. Torstensson, and K. Fujisawa, Astron. Astrophys. **539,** A79 (2012).
[18] A. G. Lyne, B. W. Stappers, M. J. Keith, P. S. Ray, M. Kerr, and F. Camilo, Mon. Not. R. Astron. Soc. **451,** 581 (2015).
[19] W. C. G. Ho, C.-Y. Ng, A. G. Lyne, B. W. Stappers, M. J. Coe, J. P. Halpern, T. J. Johnson, and I. A. Steele, Mon. Not. R. Astron. Soc. **464,** 1211 (2017).
[20] A. U. Abeysekara *et al.*, Astrophys. J. Lett. **867,** L19 (2018).
[21] M. Chernyakova, D. Malyshev, P. Blay, B. van Soelen, and S. Tsygankov, Mon. Not. R. Astron. Soc. **495,** 365 (2020).
[22] A. A. Abdo *et al.*, Astrophys. J. Lett. **658,** L33 (2007).
[23] A. Albert *et al.*, Astrophys. J. **905,** 76 (2020).
[24] E. Aliu *et al.*, Astrophys. J. **788,** 78 (2014).
[25] M. S. E. Roberts, J. W. T. Hessels, S. M. Ransom, V. M. Kaspi, P. C. C. Freire, F. Crawford, and D. R. Lorimer, Astrophys. J. Lett. **577,** L19 (2002).
[26] A. A. Abdo *et al.*, Astrophys. J. **700,** 1059 (2009).
[27] J. W. T. Hessels, M. S. E. Roberts, S. M. Ransom, V. M. Kaspi, R. W. Romani, C.-Y. Ng, P. C. C. Freire, and B. M. Gaensler, Astrophys. J. **612,** 389 (2004).
[28] A. van Etten, R. W. Romani, and C.-Y. Ng, Astrophys. J. **680,** 1417 (2008).
[29] A. Kirichenko, A. Danilenko, P. Shternin, Y. Shibanov, E. Ryspaeva, D. Zyuzin, M. Durant, O. Kargaltsev, G. Pavlov, and A. Cabrera-Lavers, Astrophys. J. **802,** 17 (2015).
[30] E. M. Levesque, P. Massey, K. A. G. Olsen, B. Plez, E. Josselin, A. Maeder, and G. Meynet, Astrophys. J. **628,** 973 (2005).
[31] N. Mauron and E. Josselin, Astron. Astrophys. **526,** A156 (2011).
[32] T. Mizuno, N. Tanaka, H. Takahashi, J. Katsuta, K. Hayashi, and R. Yamazaki, Astrophys. J. **841,** 104 (2017).
[33] E. V. Gotthelf *et al.*, Astrophys. J. **826,** 25 (2016).
[34] M. Amenomori *et al.*, Phys. Rev. Lett. **69,** 2468 (1992).
[35] M. Amenomori *et al.*, Phys. Rev. Lett. **123,** 051101 (2019).
[36] M. Amenomori *et al.*, Nat. Astron. Lett. **5,** 460 (2021).
[37] M. Amenomori *et al.*, Astrophys. J. **633,** 1005 (2005).
[38] T.-P. Li and Y.-Q. Ma, Astrophys. J. **272,** 317 (1983).
[39] A. R. Taylor *et al.*, Astron. J. **125,** 3145 (2003).
[40] I. M. Beerer *et al.*, Astrophys. J. **720,** 679 (2010).
[41] K. E. Kraemer *et al.*, Astron. J. **139,** 2319 (2010).
[42] S. Abdollahi *et al.*, Astrophys. J. Suppl. Ser. **247,** 33 (2020).
[43] K. A. van der Hucht, New Astron. Rev. **45,** 135 (2001).
[44] See the Supplemental Material at http://link.aps.org/supplemental/10.1103/PhysRevLett.127.031102 for more details on the methodology to estimate the post-trial signicance of gamma-ray detection and the analysis results above 40 TeV.
[45] G. Hobbs, D. R. Lorimer, A. G. Lyne, and M. Kramer, Mon. Not. R. Astron. Soc. **360,** 974 (2005).